Optical multiband surface photometry of a sample of Seyfert galaxies. III. Global, isophotal, and bar parameters[*]

L. Slavcheva-Mihova[**] and **B. Mihov**

Institute of Astronomy and National Astronomical Observatory, Bulgarian Academy of Sciences,
72 Tsarigradsko Chaussee Blvd., 1784 Sofia, Bulgaria

This paper is third in a series, studying the optical properties of a sample of Seyfert galaxies. Here we present a homogeneous set of global (ellipticity, position angle, inclination, and total magnitude) and isophotal (semi-major axis and colour indices at 24 V mag arcsec^{-2}) parameters of the galaxy sample. We find the following median corrected isophotal colour indices: $(B - I_{\rm C})_{24}^{(0)} = 1.9$ mag arcsec^{-2} and $(V - I_{\rm C})_{24}^{(0)} = 1.1$ mag arcsec^{-2}. A set of bar parameters – ellipticity, position angle, semi-major axis corresponding to the ellipticity maximum in the bar region, and length, are also reported; deprojection has been applied to the bar ellipticity, length, and relative length in terms of galaxy isophotal semi-major axis. Regarding bar length estimation, we use a method, based on the relation between the behaviour of the profiles and orbit analysis. The so estimated bar length tightly correlates with the semi-major axis, corresponding to the ellipticity maximum with a median ratio of the former to the latter of 1.22. The median of the deprojected bar ellipticity, length, and relative length are 0.39, 5.44 kpc, and 0.44, respectively. There is a correlation between the deprojected bar length and the corrected isophotal semi-major axis at 24 V mag arcsec^{-2}. Three of the 17 large-scale bars appear strong, based on the deprojected bar ellipticity as a first-order approximation of bar strength. The deprojected relative bar length does not appear to correlate with the bar ellipticity.

1 Introduction

The major components of disk galaxies are bulges and disks, basically different in their support against gravitational collapse (de Jong 1996a). Various correlations involving bulge and disk parameter have been established, e.g., bulge vs. disk scale lengths (MacArthur, Courteau & Holtzman 2003; Möllenhoff 2004; Aguerri et al. 2005), bulge effective surface brightness (SB) vs. Hubble type (de Jong 1996a; Möllenhoff 2004), bulge effective colour index (CI) vs. disk central CI (de Jong 1996b). Furthermore, bulge-to-disk ratio underlies morphological classification of disk galaxies. Correlations between bulge parameters and black hole mass (Ferrarese & Ford 2005) evidence the coevolution of the black hole and its host galaxy. Considering active galaxies, the problems related to the origin and angular momentum reduction mechanisms of the fuel have given rise to much discussion (e.g., Jogee 2006). In this regard, comparative analysis of the morphology and local environment of matched active and inactive galaxy samples have been performed (e.g., Mulchaey & Regan 1997; De Robertis, Yee & Hayhoe 1998; Virani, De Robertis & VanDalfsen 2000; Simões Lopes et al. 2007). Thus, studies on the fueling me-

chanisms of active galactic nuclei and correlations among galaxy parameters, as well as the precise morphological classification, all demand morphological characterization, i.e., disclosure of the features present. We analysed the evidence of non-axisymmetric perturbation of the potential in a sample of 35 Seyfert galaxies and in a matched sample of inactive galaxies, based on a detailed morphological characterization and study of the local environment. The results are presented in Slavcheva-Mihova & Mihov (2011, hereafter Paper I). Here we present a homogeneous set of global, isophotal, and bar parameters of the Seyfert galaxies[1].

Global and isophotal parameters are involved in inclination corrections and various galactic structure studies. While databases provide global and isophotal parameters for the bulk of the galaxies, they are generally based on photographic data of less photometric accuracy than CCD data.

The classical bar signature on the profiles is an ellipticity maximum, accompanied by a position angle (PA) plateau and a SB bump (Wozniak & Pierce 1991; Wozniak et al. 1995); more detailed bar criteria were introduced later on (Knapen, Shlosman & Peletier 2000; Menéndez-Delmestre et al. 2007; Marinova & Jogee 2007; Aguerri, Méndez-Abreu & Corsini 2009). There are various methods for bar length estimation, based on: visual inspection of images, analysis of the SB profile along the bar major axis, isophote fit-

---

---

[1] Three more galaxies – Mrk 1040, NGC 5506, and Mrk 507, were added.

ting with ellipses, Fourier analysis, etc. (see the reviews of Athanassoula & Misiriotis 2002; Erwin 2005; Michel-Dansac & Wozniak 2006). The semi-major axis (SMA) corresponding to the ellipticity maximum (ℓ_{max}, see Wozniak & Pierce 1991) proved to be the most robust, objective, and reproducible among the bar length estimates. It, however, underestimates bar length (Wozniak et al. 1995) and is not related to any of the bar dynamical characteristics (e.g., Michel-Dansac & Wozniak 2006). Moreover, bar strength can be defined as the maximum tangential force in terms of the mean radial force after Combes & Sanders (1981). Thus, it generally depends on the bar ellipticity, bar mass, and central force field. The tight correlation found between bar strength and deprojected bar ellipticity shows that the latter is a good measure of bar strength (Laurikainen, Salo & Rautiainen 2002). Values of the deprojected ellipticities below 0.15 are among the signatures of ovals and lenses (Kormendy & Kennicutt 2004).

Details about the sample selection, observations, data reduction, and Johnson-Cousins BVR_CI_C surface photometry, as well as contour maps and profiles of the SB, CI, ellipticity (ϵ), and PA could be found in Paper I. The extra added galaxies were reduced as the rest of sample; observational details, contour maps, and profiles are presented in Appendix A.

The paper is structured as follows. In Sect. 2 we present the global values of the ellipticity, PA, inclination, and total magnitude. The isophotal parameters – SMA and CIs at $24\ V$ mag arcsec^{-2}, are discussed in Sect. 3. The bar parameters are outlined in Sect. 4. A summary of our results is given in Sect. 5. A set of contour maps and profiles of the extra added galaxies is presented in Appendix A. Global ellipticities and deprojected bar ellipticities of the matched inactive galaxies are given in Appendix B.

Throughout the paper the linear sizes in kpc have been calculated using the cosmology-corrected scale given in NED[2] (H_0=73 km s^{-1} Mpc^{-1}, Ω_M=0.27, Ω_Λ=0.73, Spergel et al. 2007).

2 Global parameters

We present the global values of the ellipticity and PA of the sample galaxies in Table 1. They were obtained computing the median over a predefined region of the corresponding profiles; the mean absolute deviation about the median (MAD) was used as an error estimate. The region of estimations is one and the same for all passbands and epochs for a given galaxy and generally encompasses the disk-dominated parts (Table 1, see also Fig. A1 in Paper I). All available passbands were considered in the median computation for a given epoch. Multi-epoch global parameters were weight-averaged; the galaxies of multi-epoch observations can be followed in Table 3 of Paper I.

_____
[2] NASA/IPAC Extragalactic Database.

Table 1 Global values of the ellipticity, PA, and inclination, estimated over all available passbands.

Galaxy	Region[a] (arcsec)	Ellipticity	PA (degree)	Inclination (degree)
Mrk 335	10	0.09 ± 0.02	109.2 ± 13.7	25.0 ± 3.0
III Zw 2	12	0.17 ± 0.02	14.7 ± 4.7	34.7 ± 2.2
Mrk 348	20 (45)	0.09 ± 0.02	90.1 ± 41.3	25.0 ± 3.0
I Zw 1	12	0.11 ± 0.02	139.0 ± 10.9	27.7 ± 2.7
Mrk 352	7	0.21 ± 0.01	84.6 ± 1.1	38.7 ± 1.0
Mrk 573	30	0.13 ± 0.02	76.2 ± 6.8	30.2 ± 2.5
Mrk 590	15	0.06 ± 0.02	127.4 ± 14.5	20.4 ± 3.8
Mrk 1040	20	0.73 ± 0.03	74.2 ± 1.1	79.3 ± 2.8
Mrk 595	16	0.32 ± 0.01	92.3 ± 1.2	48.4 ± 0.8
3C 120	24	0.27 ± 0.02	115.0 ± 1.5	44.2 ± 1.8
Ark 120	10	0.13 ± 0.01	8.5 ± 2.3	30.2 ± 1.2
Mrk 376	11	0.29 ± 0.02	164.8 ± 2.5	45.9 ± 1.8
Mrk 79	47	0.14 ± 0.02	148.6 ± 2.5	31.4 ± 2.4
Mrk 382	17	0.16 ± 0.02	155.1 ± 6.8	33.6 ± 2.3
NGC 3227	80	0.47 ± 0.01	150.1 ± 3.1	59.9 ± 0.8
NGC 3516	35	0.19 ± 0.01	44.3 ± 4.5	36.8 ± 1.0
NGC 4051	110	0.39 ± 0.03	109.3 ± 6.3	54.0 ± 2.4
NGC 4151[b]	. . .	0.07 ± 0.03	26.0 ± 3.5	21.0 ± 5.0
Mrk 766	24	0.19 ± 0.03	66.9 ± 4.1	36.8 ± 3.2
Mrk 771	11	0.13 ± 0.01	80.2 ± 11.7	30.2 ± 1.2
NGC 4593	75	0.35 ± 0.02	70.6 ± 6.5	50.9 ± 1.6
Mrk 279	18	0.33 ± 0.01	30.8 ± 2.3	49.3 ± 0.8
NGC 5506	40	0.75 ± 0.03	87.8 ± 0.7	81.2 ± 2.8
NGC 5548	35 (60)	0.19 ± 0.01	96.2 ± 6.0	36.8 ± 1.0
Ark 479	10	0.31 ± 0.02	117.2 ± 1.5	47.6 ± 1.7
Mrk 506	12	0.27 ± 0.01	116.3 ± 2.3	44.2 ± 0.9
Mrk 507	5	0.30 ± 0.03	9.9 ± 5.8	46.8 ± 2.6
3C 382	15	0.24 ± 0.03	90.0 ± 3.3	41.6 ± 2.9
3C 390.3	8	0.12 ± 0.02	112.7 ± 9.9	29.0 ± 2.6
NGC 6814	60	0.08 ± 0.01	92.2 ± 17.8	23.6 ± 1.6
Mrk 509	8	0.16 ± 0.02	72.4 ± 3.6	33.6 ± 2.3
Mrk 1513	13	0.54 ± 0.01	57.9 ± 1.2	65.0 ± 0.7
Mrk 304	6	0.03 ± 0.01	54.5 ± 26.5	14.4 ± 2.6
Ark 564	16	0.22 ± 0.01	112.2 ± 1.9	39.7 ± 1.0
NGC 7469	50	0.26 ± 0.01	124.4 ± 1.5	43.4 ± 0.9
Mrk 315	13	0.14 ± 0.01	33.2 ± 5.4	31.4 ± 1.2
NGC 7603	18	0.32 ± 0.01	166.8 ± 2.9	48.4 ± 0.8
Mrk 541	20	0.36 ± 0.01	172.3 ± 1.3	51.6 ± 0.8

[a] Start SMA, defining the region, over which the global values of the ellipticity and PA were estimated. The region generally extends to the profile end with two exceptions, for which the end SMA is given in parentheses.
[b] The global parameters were taken from Simkin (1975).

Having estimated the ellipticity, we obtained the galaxy inclination, i, using the expression (Holmberg 1958):

$$\cos i = \sqrt{\frac{(1-\epsilon)^2 - q_0^2}{1 - q_0^2}},$$

where $q_0 = 0.2$ is the intrinsic, edge-on disk axial ratio (Lambas, Maddox & Loveday 1992). The so derived inclination is presented in Table 1. The outermost, disk-dominated, parts of NGC 4151 could not be reached in our images, so, we list the parameters estimated by Simkin (1975).
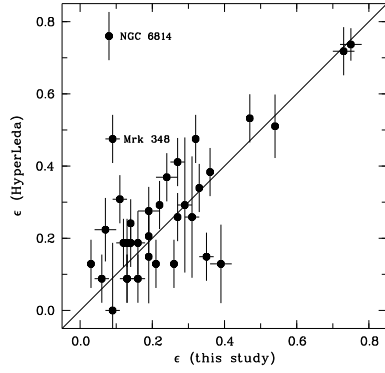
Fig. 1 Comparison between the ellipticities listed in HyperLeda and ours. Named are the galaxies with $|\Delta\epsilon| > 0.3$. The line of exact correspondence is plotted.
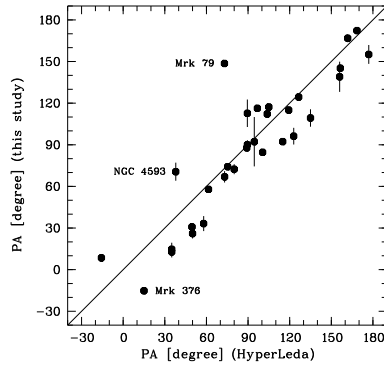

Fig. 2 Comparison between the PAs listed in HyperLeda and ours. Named are the galaxies with $|\Delta PA| > 30°$. The line of exact correspondence is plotted.
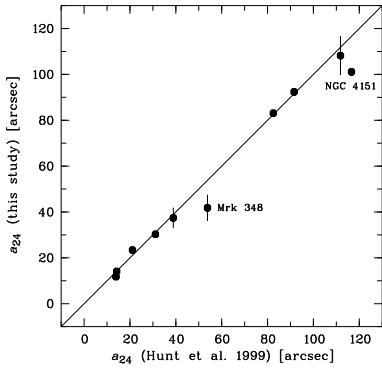

Fig. 3 Comparison between a_{24} estimated by us and those published in Hunt et al. (1999). Named are the outliers. The line of exact correspondence is plotted.
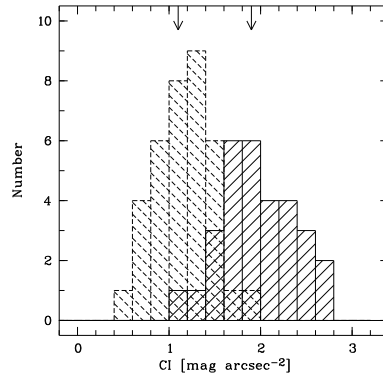

Fig. 4 Distribution of $(B-I_{\rm C})_{24}^{(0)}$ (solid) and $(V-I_{\rm C})_{24}^{(0)}$ (dashed), whose median values are denoted by the right and left arrow, respectively.
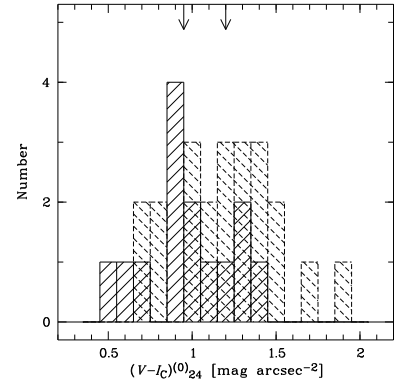

Fig. 5 Distribution of $(V-I_{\rm C})_{24}^{(0)}$ for the galaxies with/without outer rings (solid/dashed) with the median values denoted by the left/right arrow.

The typical error of the global PA is a few degrees, but it may get higher for nearly face-on galaxies ($\epsilon \lesssim 0.1$) as no favourable PA could be defined (e.g., Mrk 590, see Paper I) and owing to the presence of spiral arms as they can lead to a continuous PA change (e.g., Mrk 348, see Paper I). We found good passband-to-passband and night-to-night correspondence of the global ellipticities and PAs as can be judged by the small values of the errors reported in Table 1.

We compared the values of the global ellipticity and PA with those listed in HyperLeda[3] (Paturel et al. 2003) in Figs. 1 and 2; note that HyperLeda reports the parameters corresponding to the 25 B mag arcsec^{-2} isophote. The median values of the difference of the ellipticity and PA (ours minus theirs) are -0.02 (0.10) and $-4°.3$ (15°.8), respectively, with MAD in parentheses. Two galaxies have ellipticity difference $|\Delta\epsilon| > 0.3$ – NGC 6814 and Mrk 348. The former, practically a face-on galaxy, is reported to have $\epsilon = 0.76$. The latter is also an almost face-on galaxy with a

stretched spiral structure beyond $a \approx 40''$, where the 25 B mag arcsec^{-2} isophote gets (see Fig. A.1 of Paper I). Similar is the case of Mrk 79, at the top of the list of galaxies with PA difference $|\Delta PA| > 30°$ – the 25 B mag arcsec^{-2} isophote falls in the region of a continuous PA change owing to the spiral arms (see Fig. A.1 of Paper I). Thus, the relatively large scatter in Figs. 1 and 2 is associated with the different way of estimation of these parameters. Furthermore, the ellipticity (together with inclination) and PA, estimated on the base of isophotal criteria, are not fully representative for the disk-dominated galaxy regions.

The global ellipticities of the matched inactive galaxies are presented in Appendix B.

We built the growth curve for each galaxy by integrating the intensity in elliptical apertures of fixed centre, ellipticity, and PA, using the global ellipticity and PA. The intensity, at which the growth curve becomes asymptotically flat, specifies the total apparent magnitude, presented in Table 2. The total magnitude error includes photon noise, sky back-

---

[3] http://leda.univ-lyon1.fr

ground error, and transformation coefficient errors. No magnitude averaging was performed, so that eventual changes related to nuclear variability could remain.

3   Isophotal parameters

In Table 3 we present a set of 24 V mag arcsec^{-2} isophote parameters: the SMA a_{24} together with the CIs $(B-I_{\rm C})_{24}$ and $(V-I_{\rm C})_{24}$ estimated on both the apparent, $\mu(a)$, and corrected, $\mu^{(0)}(a)$, SB profiles; the superscript "0" denotes the corrected quantities. Correction was performed as follows:

$$\mu^{(0)}(a) = \mu(a) - \Sigma,$$

where

$$\Sigma = A + 2.5\,C\log(\cos i) + 10\log(1+z) + K + E$$

accounts for the following factors:

– *Galactic absorption, A.* Its values calculated following Schlegel, Finkbeiner & Davis (1998) were taken from NED;
– *Correction for inclination and internal absorption.* Factor C accounts for the disk transparency owing to dust absorption. It depends on the radial distance and is assumed to vary from about 0 in the disk centre to about 1 in the galaxy outskirts (e.g., Giovanelli et al. 1994). For the sake of estimating the 24 V mag arcsec^{-2} parameters, we adopted $C = 0.9$ (Nedyalkov 1998);
– *Cosmological dimming*;
– *K- and E-correction.* We used the following fits to the data points with $z \leq 0.1$ and Hubble type Sa of Poggianti (1997):

$$\begin{aligned} K_B &= 4.290\,z, \\ K_V &= 1.370\,z, \\ K_I &= -0.014\,z + 1.786\,z^2, \end{aligned}$$

and

$$\begin{aligned} E_B &= -2.470\,z, \\ E_V &= -1.945\,z, \\ E_I &= -1.615\,z. \end{aligned}$$

Poggianti (1997) did not tabulate K- and E-corrections for Sa in the Cousins I, so, we used the corrections for the Johnson I.

When the 24 V mag arcsec^{-2} isophote could not be reached, extrapolation, instead of interpolation, was performed on the base of a linear fit to the disk-dominated galaxy regions, using the following formula (Han 1992):

$$a_{24}^{\rm (x)} = (24 - \mu_0)\,\frac{r_0}{1.0857},$$

where $a_{24}^{\rm (x)}$ is the extrapolated a_{24} and μ_0 and r_0 the central SB and the scale length of the fitted galaxy disk, respectively. In case the CI profiles do not reach a_{24}, linear fits to the corresponding SB profiles were used to extrapolate

them. The multi-epoch isophotal parameters were weight-averaged.

Our values of a_{24} are in good agreement with those of Hunt et al. (1999) for the galaxies in common (Fig. 3). The median value of the difference (ours minus theirs) is $-1\rlap{.}{''}2$ with MAD of $3\rlap{.}{''}8$. The outliers are Mrk 348 and NGC 4151. Possible reasons for this are eventual differences in the sky background estimation and that, at variance with us, Hunt et al. (1999) used fixed values of the ellipticity and PA in the ellipse fitting in the region of the 24 V mag arcsec^{-2} isophote for most galaxies, including the above cited. Note also that in this region the SB profile of Mrk 348 has an almost flat appearance (see Fig. A1 in Paper I), which results in a relatively large error in the estimation of a_{24} and that Hunt et al. (1999) applied extrapolation to estimate a_{24} of NGC 4151.

The median corrected isophotal SMA is 13.9 kpc with MAD of 3.7 kpc. The distribution of the corrected CIs is shown in Fig. 4. We acquired the following median CIs:

$$\begin{aligned} (B-I_{\rm C})_{24} &= 2.2\,(0.4)\,{\rm mag\,arcsec}^{-2}, \\ (V-I_{\rm C})_{24} &= 1.3\,(0.2)\,{\rm mag\,arcsec}^{-2}, \\ (B-I_{\rm C})_{24}^{(0)} &= 1.9\,(0.3)\,{\rm mag\,arcsec}^{-2}, \\ (V-I_{\rm C})_{24}^{(0)} &= 1.1\,(0.3)\,{\rm mag\,arcsec}^{-2}, \end{aligned}$$

which are representative for the disk-dominated galaxy regions; the values in parentheses are the MADs.

We compared the distribution of the corrected CIs in the subsamples that have bars, outer/inner rings, asymmetries, companions and in the corresponding subsamples without these features. The subsample with outer rings shows bluer CIs than the complementary subsample at more than the 95% significance level. In particular, the median $(V-I_{\rm C})_{24}^{(0)}$ of the subsample with/without outer rings is 0.95/1.20 mag arcsec^{-2} (Fig. 5). This is expected, since outer rings, typically blue, are generally situated close to the 24 V mag arcsec^{-2} isophote. There is no clear correlation between the CIs and the presence of the other features.

4   Bar parameters

We consider a galaxy barred if there is an ellipticity maximum greater than 0.16 with an amplitude of at least 0.08 over a region of PA constant within $20°$, following Aguerri et al. (2009). At the transition to the disk the PA changes unless the bar and disk are aligned.

The ellipticity maximum and the corresponding PA in the region of the bar are adopted as its ellipticity ($\epsilon_{\rm bar}$) and PA ($PA_{\rm bar}$), respectively. The presence of a bulge, together with eventual boxiness of the bar isophotes, leads to underestimation of the bar ellipticity, obtained on the base of ellipse fits, especially in galaxies with big bulges (see also Menéndez-Delmestre et al. 2007). Generally, the PA along bars is well constrained thanks to the x_1 orbits (e.g., Athanassoula 1992).
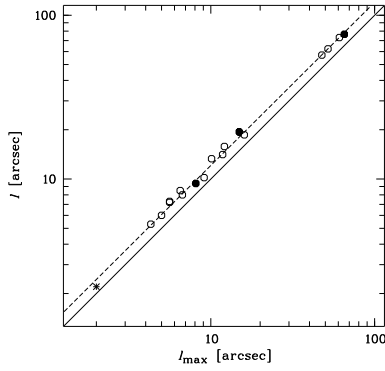
Fig. 6 Bar length vs. bar SMA at ellipticity maximum of strong (filled circles) and weak (open circles) bars; the nuclear bar of Mrk 352 is denoted by an asterisk. Overplotted are the lines of the median $\ell/\ell_{\max}$ ratio (dashed) and of exact correspondence (solid).
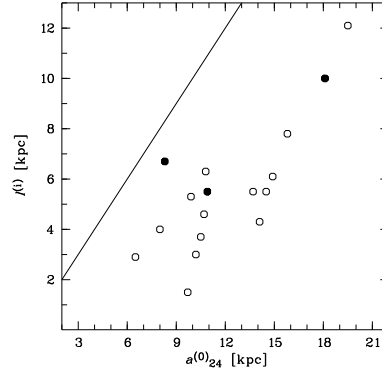
Fig. 7 Deprojected bar length vs. corrected isophotal SMA at 24 V mag arcsec^{-2}; the symbols are as specified in Fig. 6. Overplotted is the line of exact correspondence.
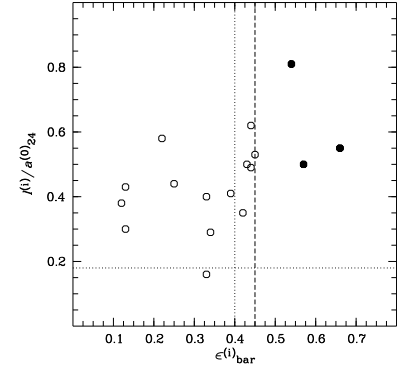
Fig. 8 Deprojected relative bar length vs. deprojected bar ellipticity; the symbols are as specified in Fig. 6. Overplotted are empirical limits of strong and long bars (see text).

As bar length, ℓ, we adopted the SMA, where the ellipticity decreases with 15% from its maximal value, after Martinez-Valpuesta, Shlosman & Heller (2006), according to whom the so estimated length is consistent with the size of the maximal stable x_1 orbit; bar length has already been derived in that manner by Fathi et al. (2009). The post-maximum ellipticity slope, generally steeper than the pre-maximum one, is often influenced by spiral arm beginnings or rings. To reduce this influence, we took the minimum of the SMAs, corresponding to the 15% ellipticity decrease, both before and after the ellipticity maximum. The error of ℓ and $\ell_{\max}$ was estimated as the SMA change relevant to $1\,\sigma$ change of the corresponding ellipticity.

This approach worked well for all barred galaxies[4] but NGC 3227, NGC 4051, and NGC 4593, for which it overestimates the bar lengths. Not taking these galaxies into account, we found ℓ and $\ell_{\max}$ to correlate tightly (with a Pearson correlation coefficient of 0.999 and a probability that this is achieved by uncorrelated points below 10^{-6}, Fig. 6). The median value of the ratio $\ell/\ell_{\max}$ is 1.22 with a MAD of 0.06. The bar lengths of the above three galaxies were estimated using the corresponding $\ell_{\max}$ values and the median $\ell/\ell_{\max}$ ratio.

We used the $I_{\rm C}$ profiles to estimate the bar parameters as bars are best pronounced and the spiral structure influence is minimized there. The derived parameters are listed in Table 4; multi-epoch bar parameters were weight-averaged except for Mrk 79[5]. The bar parameters of Mrk 352, Mrk 771, and Mrk 279 were estimated using Hubble Space Telescope

(HST) data and the ones of NGC 6814 – using Two Micron All Sky Survey (2MASS) data (see Paper I).

The bar length was deprojected following Martin (1995):

$$\ell^{(i)} = \ell\sqrt{\cos^2\Theta + \sec^2 i\,\sin^2\Theta}\,,$$

where Θ is the angle between the SMAs of the bar and disk. To compute the deprojected bar ellipticity, $\epsilon_{\rm bar}^{(i)}$, the bar semi-minor axis was deprojected using the above formula, multiplied by $1-\epsilon_{\rm bar}$; now Θ is the angle between the semi-minor axis of the bar and the SMA of the disk.

The median of the deprojected bar ellipticity, length, and relative length, $\ell^{(i)}/a_{24}^{(0)}$, are 0.39 (0.12), 5.44 (1.80) kpc, and 0.44 (0.11), respectively, with the corresponding MADs given in parentheses.

Figure 7 shows $\ell^{(i)}$ as a function of $a_{24}^{(0)}$, the Pearson correlation coefficient is 0.783 (with a probability that this is achieved by uncorrelated points about 10^{-4}); a weaker correlation was found by Laine et al. (2002).

Deprojected bar ellipticity can be used as a first-order approximation of bar strength (e.g., Laurikainen et al. 2002; Block et al. 2004). We classified a bar as strong if $\epsilon_{\rm bar}^{(i)} > 0.45$ after Laine et al. (2002). This resulted in three strong bars among the 17 barred galaxies. In particular, Seyfert bars appear weaker than their inactive counterparts at the 95% confidence level (see Paper I). The deprojected bar ellipticities of the matched inactive sample used in this comparison are listed in Appendix B. Concerning the morphological classification presented in Paper I, the barred galaxies of both samples were given designations "AB" or "B" according to the values of their deprojected ellipticities.

The bar-like structures of Mrk 595, Mrk 279, and NGC 7469 are most probably ovals/lenses, given their deprojected ellipticities below 0.15 (Kormendy & Kennicutt 2004); to further specify this, kinematic data are needed though

---

[4] We consider only large-scale bars. Given also in Table 4 are the parameters of the nuclear bar of Mrk 352, firstly reported in Paper I, but they were not taken into account in any of the correlations below, nor in the estimation of the median parameters.

[5] Only the data of better seeing were taken into account (see Paper I).

(Sellwood & Wilkinson 1993). Note that bars, ovals, and lenses are essentially equivalent regarding gas inflow (Kormendy & Kennicutt 2004).

The deprojected relative bar length and bar ellipticity show no clear correlation (Fig. 8; see also Fig. 5 of Márquez et al. 2000 and Fig. 6 of Laine et al. 2002). Overplotted are the empirical limits of long ($\ell^{(i)}/a_{24}^{(0)} \geq 0.18$) and strong ($\epsilon \geq 0.4$) bars of Martinet & Friedli (1997)[6], dotted, and of strong bars ($\epsilon > 0.45$) of Laine et al. (2002), dashed.

5 Summary

This paper is third in a series, studying the optical properties of a sample of Seyfert galaxies. The first paper addresses the evidence of non-axisymmetric perturbation of the potential in a sample of 35 Seyfert galaxies and in a matched inactive sample. A homogeneous set of global (ellipticity, PA, inclination, and total magnitude) and isophotal (SMA and CIs at 24 V mag arcsec^{-2}) parameters of the Seyfert sample are reported in this study. Correction for galactic absorption, inclination and internal absorption, cosmological dimming, as well as K- and E-correction was applied to the isophotal parameters. We found the following median isophotal parameters:

$$
\begin{aligned}
a_{24}^{(0)} &= 13.9\,\mathrm{kpc}, \\
(B - I_{\mathrm{C}})_{24} &= 2.2\,\mathrm{mag\,arcsec}^{-2}, \\
(V - I_{\mathrm{C}})_{24} &= 1.3\,\mathrm{mag\,arcsec}^{-2}, \\
(B - I_{\mathrm{C}})_{24}^{(0)} &= 1.9\,\mathrm{mag\,arcsec}^{-2}, \\
(V - I_{\mathrm{C}})_{24}^{(0)} &= 1.1\,\mathrm{mag\,arcsec}^{-2}.
\end{aligned}
$$

The estimated parameters can be further used in various galactic structure studies.

We presented a set of bar parameters – ellipticity, PA, SMA corresponding to the ellipticity maximum in the bar region, and length; deprojected values of the bar ellipticity, length, and relative length in terms of galaxy isophotal SMA are also given. As bar length we adopted the minimum of the SMAs corresponding to 15% ellipticity decrease from its maximal value, both before and after the ellipticity maximum. The so obtained bar length and the most often used bar length estimate – the SMA, corresponding to the ellipticity maximum, show a tight correlation with a median ratio $\ell/\ell_{\max}$ of 1.22, which we further used to obtain the bar length in cases the above approach did not work. The median of the deprojected bar ellipticity, length, and relative length are 0.39, 5.44 kpc, and 0.44, respectively. The deprojected bar length correlates with the corrected isophotal SMA at 24 V mag arcsec^{-2}. Seventeen of the galaxies have large-scale bars, three of which are strong, based on the deprojected bar ellipticity as a rough estimate of bar strength. The deprojected relative bar length and bar ellipticity show no clear correlation.

---

[6] Note that our definition of bar length differs from that used by the authors.

Global ellipticities and deprojected bar ellipticities of the matched inactive sample are also presented.

References

Aguerri, J. A. L., Elias-Rosa, N., Corsini, E. M., Muñoz-Tuñón, C.: 2005, A&A 434, 109

Aguerri, J. A. L., Méndez-Abreu, J., Corsini, E. M.: 2009, A&A 495, 491

Athanassoula, E.: 1992, MNRAS 259, 345

Athanassoula, E., Misiriotis, A.: 2002, MNRAS 330, 35

Block, D. L., Buta, R., Knapen, J. H., Elmegreen, D. M., Elmegreen, B. G., Puerari, I.: 2004, AJ 128, 183

Chatzichristou, E. T.: 2000, ApJS 131, 71

Combes, F., Sanders, R. H.: 1981, A&A 96, 164

de Jong, R. S.: 1996a, A&A 313, 45

de Jong, R. S.: 1996b, A&A 313, 377

De Robertis, M. M., Yee, H. K. C., Hayhoe, K.: 1998, ApJ 496, 93

Erwin, P.: 2005, MNRAS 364, 283

Fathi, K., Beckman, J. E., Piñol-Ferrer, N., Hernandez, O., Martínez-Valpuesta, I., Carignan, C.: 2009, ApJ 704, 1657

Ferrarese, L., Ford, H.: 2005, Space Sci. Rev. 116, 523

Gioia, I. M., Henry, J. P., Mullis, C. R., Böhringer, H., Briel, U. G., Voges, W., Huchra, J. P.: 2003, ApJS 149, 29

Giovanelli, R., Haynes, M. P., Salzer, J. J., Wegner, G., da Costa, L. N., Freudling, W.: 1994, AJ 107, 2036

Halpern, J. P., Oke, J. B.: 1987, ApJ 312, 91

Han, M.: 1992, ApJS 81, 35

Holmberg, E.: 1958, Lund Medd. Astron. Obs. Ser. II 136, 1

Hunt, L. K., Malkan, M. A., Rush, B., Bicay, M. D., Nelson, B. O., Stanga, R. M., Webb, W.: 1999, ApJS 125, 349

Jogee, S.: 2006, Physics of Active Galactic Nuclei at all Scales, eds. D. Alloin, R. Johnson, P. Lira, LNP 693, 143

Knapen, J. H., Shlosman, I., Peletier, R. F.: 2000, ApJ 529, 93

Kormendy, J., Kennicutt Jr., R. C.: 2004, ARA&A 42, 603

Laine, S., Shlosman, I., Knapen, J. H., Peletier, R. F.: 2002, ApJ 567, 97

Lambas, D. G., Maddox, S. J., Loveday, J.: 1992, MNRAS 258, 404

Laurikainen, E., Salo, H., Rautiainen, P.: 2002, MNRAS 331, 880
MacArthur, L. A., Courteau, S., Holtzman, J. A.: 2003, ApJ 582, 689
Marinova, I., Jogee, S.: 2007, ApJ 659, 1176
Márquez, I., Durret, F., Masegosa, J., et al.: 2000, A&A 360, 431
Martin, P.: 1995, AJ 109, 2428
Martinet, L., Friedli, D.: 1997, A&A 323, 363
Martinez-Valpuesta, I., Shlosman, I., Heller, C.: 2006, ApJ 637, 214
Menéndez-Delmestre, K., Sheth, K., Schinnerer, E., Jarrett, T. H., Scoville, N. Z.: 2007, ApJ 657, 790
Michel-Dansac, L., Wozniak, H.: 2006, A&A 452, 97
Möllenhoff, C.: 2004, A&A 415, 63
Mulchaey, J., Regan, M.: 1997, ApJ 482, L135
Nedyalkov, P.: 1998, Observational manifestation of the extinction in disks of spiral galaxies (PhD thesis), Department of Astronomy, University of Sofia
Paturel, G., Petit, C., Prugniel, P., Theureau, G., Rousseau, J., Brouty, M., Dubois, P., Cambrésy, L.: 2003, A&A 412, 45
Poggianti, B. M.: 1997, A&AS 122, 399
Schlegel, D. J., Finkbeiner, D. P., Davis, M.: 1998, ApJ 500, 525
Sellwood, J. A., Wilkinson, A.: 1993, Rep. Prog. Phys. 56, 173
Simkin, S. M.: 1975, ApJ 200, 567
Simões Lopes, R. D., Storchi-Bergmann, T., de Fátima, S. M., Martini, P.: 2007, ApJ 655, 718
Slavcheva-Mihova, L., Mihov, B.: 2011, A&A 526, A43 (Paper I)
Spergel, D. N., Bean, R., Doré, O., et al.: 2007, ApJS 170, 377
Virani, S. N., De Robertis, M. M., VanDalfsen, M. L.: 2000, AJ 120, 1739
Wozniak, H., Pierce, M. J.: 1991, A&AS 88, 325
Wozniak, H., Friedli, D., Martinet, L., Martin, P., Bratschi, P.: 1995, A&AS 111, 115

A   Details about the galaxies Mrk 1040, NGC 5506, and Mrk 507

The galaxies were observed at the Rozhen National Astronomical Observatory, Bulgaria, with the 2-m Ritchey-Chrétien telescope equipped with 1024×1024 Photometrics AT200 CCD camera (CCD chip SITe SI003AB with a square pixel size of $24\,\mu$m that corresponds to $0''.309$ on the sky). Standard Johnson-Cousins $BVR_{\mathrm{C}}I_{\mathrm{C}}$ filters were used. We present details about the observations, image quality, and standard fields used for calibration of the extra added galaxies in Table A1. Calibrated contour maps and profiles of the SB, CI, ellipticity, and PA are given in Fig. A1. Regarding Mrk 507, a stellar-like object (Halpern & Oke 1987; Gioia et al. 2003) of comparable brightness is located about $2''$ from its nucleus at $\mathrm{PA} = 110°$. We cleaned the projected object with the help of Moffat PSF subtraction; we should, however, keep in mind the close proximity of the object and the small size of the galaxy itself.

B   Global ellipticities and deprojected bar ellipticities of the matched inactive galaxies

We present the global ellipticities of the inactive galaxies and the deprojected bar ellipticities of the barred subsample in Table B1. Both sets of ellipticities were estimated as for the Sy sample. The median of the deprojected bar ellipticity is 0.49 with a MAD of 0.14. The galaxy ellipticities were used in the sample matching,

Table B1   Global ellipticities, estimated over all available passbands, and deprojected bar ellipticities, determined in the reddest available passband, of the matched inactive galaxies.

Seyfert	Inactive	ϵ	$\epsilon_{\mathrm{bar}}^{(i)}$
Mrk 335	IC 5017	0.18	0.55
III Zw 2	2MASX J01505708+0014040	0.30	…
Mrk 348	NGC 2144	0.16	…
I Zw 1	ESO 155– G 027	0.07	0.68
Mrk 352	2MASX J04363658–0250350	0.26	…
Mrk 573	ESO 542– G 015	0.08	0.29
Mrk 590	NGC 4186	0.20	…
Mrk 595	2MASX J00342513–0735582	0.42	0.14
3C 120	ESO 202– G 001	0.39	…
Ark 120	IC 5065	0.10	0.12
Mrk 376	ESO 545– G 036	0.12	…
Mrk 79	ESO 340– G 036	0.13	0.51
Mrk 382	ESO 268– G 032	0.26	0.44
NGC 3227	IC 5240	0.27	0.64
NGC 3516	ESO 183– G 030	0.20	…
NGC 4051	IC 1993	0.05	…
NGC 4151	NGC 2775	0.20	…
Mrk 766	UGC 6520	0.32	0.47
Mrk 771	ESO 349– G 011	0.26	0.56
NGC 4593	NGC 4902	0.07	0.58
Mrk 279	ESO 324– G 003	0.31	…
NGC 5548	NGC 466	0.12	…
Ark 479	ESO 297– G 027	0.42	…
Mrk 506	ESO 510– G 048	0.38	…
3C 382	ESO 292– G 022	0.34	…
3C 390.3	ESO 249– G 009	0.15	0.37
NGC 6814	NGC 7421	0.20	0.57
Mrk 509	ESO 147– G 013	0.15	…
Mrk 1513	2MASX J14595983+2046121	0.61	…
Mrk 304	ESO 292– G 007	0.36	…
Ark 564	ESO 552– G 053	0.14	0.69
NGC 7469	NGC 897	0.32	…
Mrk 315	ESO 423– G 016	0.16	0.36
NGC 7603	ESO 113– G 050	0.36	…
Mrk 541	UGC 9532 NED04	0.29	0.40

and the bar ellipticities were involved in the bar strength comparison of the two samples (see Paper I).
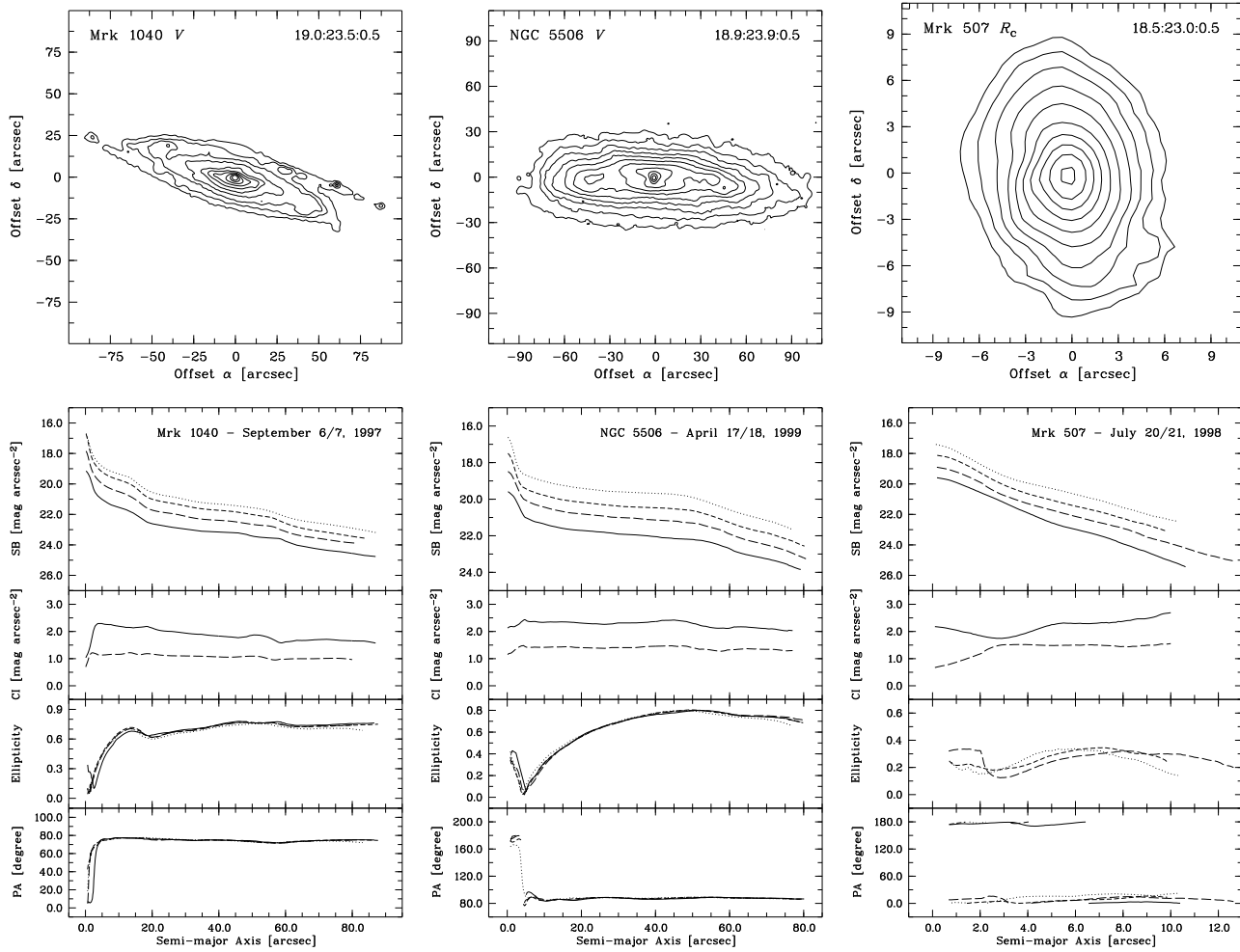
Fig. A1   Calibrated contour maps and profiles of the extra added galaxies, ordered by right ascension. Upper panels: contour maps. North is up and east to the left. The galaxy names and passbands are denoted in the upper left; the numbers in the upper right denote the start SB, end SB, and SB step in units of mag arcsec^{-2}. Lower panels: Profiles of the SB, CI, ellipticity, and PA. The CI profiles shown are $B - I_C$ (solid) and $V - I_C$ (dashed). For the rest of the profiles the solid, long-dashed, short-dashed, and dotted line is for the B-, V-, R_C-, and I_C-band, respectively.

Table 2 Total magnitudes.

Galaxy	Civil Date (yyyy mm dd)	$B_{\rm tot}$ (mag)	$V_{\rm tot}$ (mag)	$R_{\rm C,tot}$ (mag)	$I_{\rm C,tot}$ (mag)
Mrk 335	1998 08 22	14.19 ± 0.03	13.93 ± 0.03	13.47 ± 0.03	13.08 ± 0.05
	2007 08 20	. . .	14.02 ± 0.02	13.59 ± 0.02	13.30 ± 0.04
III Zw 2	1997 09 09	15.85 ± 0.05	14.86 ± 0.04	14.39 ± 0.02	13.79 ± 0.05
Mrk 348	1997 09 07	13.79 ± 0.05	12.90 ± 0.04	12.38 ± 0.04	11.86 ± 0.04
I Zw 1	1998 08 20	14.48 ± 0.05	14.06 ± 0.05	13.64 ± 0.05	13.15 ± 0.06
Mrk 352	2007 08 21	. . .	. . .	13.82 ± 0.01	. . .
	2008 01 30	15.38 ± 0.01	14.57 ± 0.02	13.99 ± 0.02	13.42 ± 0.03
Mrk 573	1997 09 07	13.97 ± 0.06	13.17 ± 0.04	12.67 ± 0.04	12.07 ± 0.05
Mrk 590	1997 09 06	13.23 ± 0.03	12.52 ± 0.03	11.98 ± 0.03	11.28 ± 0.04
Mrk 1040	1997 09 06	13.65 ± 0.03	12.80 ± 0.03	12.19 ± 0.03	11.73 ± 0.04
Mrk 595	1997 09 09	15.12 ± 0.05	14.29 ± 0.03	13.61 ± 0.03	12.92 ± 0.05
3C 120	1997 09 09	14.55 ± 0.04	13.86 ± 0.03	13.19 ± 0.03	12.51 ± 0.05
	2008 02 01	14.34 ± 0.04	13.75 ± 0.03	13.24 ± 0.03	12.69 ± 0.02
Ark 120	1994 09 29	13.97 ± 0.07	. . .	12.89 ± 0.03	. . .
	1991 12 08	. . .	13.45 ± 0.05	. . .	. . .
Mrk 376	2008 02 03	15.21 ± 0.05	14.62 ± 0.07	13.86 ± 0.03	13.33 ± 0.04
Mrk 79	1999 02 16	13.72 ± 0.03	13.08 ± 0.03	12.48 ± 0.03	11.91 ± 0.05
	2008 02 01	13.85 ± 0.03	13.14 ± 0.03	12.65 ± 0.04	12.12 ± 0.04
Mrk 382	1998 02 27	15.30 ± 0.03	14.63 ± 0.03	14.09 ± 0.04	13.56 ± 0.05
	2008 02 02	15.21 ± 0.03	14.63 ± 0.03	14.11 ± 0.03	13.58 ± 0.03
NGC 3227	1999 04 17	11.62 ± 0.07	10.84 ± 0.05	10.23 ± 0.06	9.43 ± 0.06
NGC 3516	2008 01 08	. . .	11.65 ± 0.01	11.13 ± 0.01	10.55 ± 0.01
NGC 4051	1995 05 06	11.09 ± 0.01	. . .	. . .	. . .
	2000 03 30	. . .	. . .	9.78 ± 0.02	. . .
	2001 04 09	. . .	. . .	. . .	9.18 ± 0.02
NGC 4151	1999 03 10	11.13 ± 0.03	10.52 ± 0.04	10.00 ± 0.04	9.33 ± 0.05
	1999 04 19	11.25 ± 0.05	10.56 ± 0.04	10.05 ± 0.04	9.45 ± 0.05
Mrk 766	1999 02 15	13.83 ± 0.07	13.10 ± 0.03	12.58 ± 0.04	11.97 ± 0.06
Mrk 771	1990 06 23	. . .	14.37 ± 0.03	. . .	13.11 ± 0.01
NGC 4593	2008 01 08	. . .	11.11 ± 0.01	10.59 ± 0.01	10.00 ± 0.01
Mrk 279	2008 02 02	14.43 ± 0.04	13.76 ± 0.03	13.23 ± 0.04	12.79 ± 0.06
NGC 5506	1999 04 17	12.59 ± 0.07	11.91 ± 0.05	11.16 ± 0.06	10.34 ± 0.06
NGC 5548	1999 04 19	12.76 ± 0.05	12.27 ± 0.04	11.79 ± 0.05	11.18 ± 0.06
Ark 479	2007 07 19	. . .	14.62 ± 0.06	14.05 ± 0.07	13.48 ± 0.08
Mrk 506	1997 06 01	15.09 ± 0.04	14.29 ± 0.04	13.76 ± 0.05	13.01 ± 0.05
	1998 07 18	15.01 ± 0.04	14.20 ± 0.02	13.62 ± 0.03	12.99 ± 0.05
	2007 06 17	15.38 ± 0.03	14.33 ± 0.02	13.82 ± 0.03	. . .
Mrk 507	1998 07 20	16.77 ± 0.06	15.85 ± 0.05	15.21 ± 0.05	14.23 ± 0.06
3C 382	1998 08 23	14.18 ± 0.04	13.85 ± 0.04	13.31 ± 0.04	12.78 ± 0.05
3C 390.3	1998 08 20	15.93 ± 0.06	15.05 ± 0.04	14.40 ± 0.04	13.93 ± 0.05
NGC 6814	1997 07 06	12.16 ± 0.02	11.30 ± 0.02	10.37 ± 0.02	9.62 ± 0.03
	1997 07 10	12.30 ± 0.03	11.36 ± 0.02	10.56 ± 0.03	9.69 ± 0.04
	1997 09 07	12.14 ± 0.05	11.10 ± 0.03	10.36 ± 0.03	9.49 ± 0.04
	1998 07 18	12.28 ± 0.04	11.26 ± 0.02	10.54 ± 0.03	9.79 ± 0.05
Mrk 509	1997 07 10	14.09 ± 0.03	13.59 ± 0.02	13.08 ± 0.03	12.65 ± 0.04
	1997 09 08	13.89 ± 0.03	13.48 ± 0.02	12.99 ± 0.03	12.69 ± 0.04
	1998 07 20	13.40 ± 0.05	13.16 ± 0.04	12.70 ± 0.04	12.30 ± 0.05
Mrk 1513	2007 08 20	. . .	14.54 ± 0.02	14.08 ± 0.02	13.79 ± 0.01
Mrk 304	1998 07 19	14.61 ± 0.04	14.31 ± 0.03	13.82 ± 0.03	13.50 ± 0.04
Ark 564	1998 07 18	14.22 ± 0.04	13.71 ± 0.02	13.27 ± 0.03	12.97 ± 0.04
	1998 08 20	14.34 ± 0.05	13.82 ± 0.04	13.37 ± 0.04	12.90 ± 0.05
NGC 7469	1997 09 06	12.73 ± 0.03	12.17 ± 0.03	11.67 ± 0.02	11.01 ± 0.04
	1998 07 19	12.70 ± 0.04	12.18 ± 0.03	11.77 ± 0.03	11.11 ± 0.04
	1998 08 23	12.87 ± 0.04	12.40 ± 0.04	11.80 ± 0.04	11.05 ± 0.05
	2003 07 28	13.33 ± 0.03	12.42 ± 0.03	11.75 ± 0.02	11.45 ± 0.03
Mrk 315	2007 08 22	. . .	. . .	13.89 ± 0.03	. . .
NGC 7603	2007 07 19	. . .	12.47 ± 0.07	. . .	11.51 ± 0.08
Mrk 541	2007 07 19	. . .	14.73 ± 0.07	14.12 ± 0.07	13.52 ± 0.08

Table 3   Apparent and corrected SMA and CIs at 24 V mag arcsec^{-2}.

Galaxy	a_{24} (arcsec)	$(B - I_{\mathrm{C}})_{24}$ (mag arcsec^{-2})	$(V - I_{\mathrm{C}})_{24}$ (mag arcsec^{-2})	$a_{24}^{(0)}$ (kpc)	$(B - I_{\mathrm{C}})_{24}^{(0)}$ (mag arcsec^{-2})	$(V - I_{\mathrm{C}})_{24}^{(0)}$ (mag arcsec^{-2})
Mrk 335	11.8 ± 0.7	2.3 ± 0.3	1.5 ± 0.3	5.9 ± 0.4	2.1 ± 0.3	1.4 ± 0.3
III Zw 2	10.8 ± 0.5	3.2 ± 0.2	1.6 ± 0.2	20.5 ± 1.8	2.7 ± 0.2	1.4 ± 0.2
Mrk 348	41.8 ± 5.7	1.8 ± 0.3	0.9 ± 0.2	15.5 ± 4.3	1.6 ± 0.3	0.8 ± 0.2
I Zw 1	14.1 ± 0.7	2.1 ± 0.2	1.3 ± 0.2	17.0 ± 0.8	1.8 ± 0.2	1.1 ± 0.2
Mrk 352	15.6 ± 0.5	2.2 ± 0.3	1.3 ± 0.2	4.2 ± 0.1	2.0 ± 0.3	1.2 ± 0.2
Mrk 573	33.3 ± 1.7	1.9 ± 0.4	1.0 ± 0.2	10.5 ± 0.6	1.7 ± 0.4	0.9 ± 0.2
Mrk 590	40.2 ± 1.8	2.9 ± 0.3	1.3 ± 0.2	20.8 ± 0.9	2.7 ± 0.3	1.3 ± 0.2
Mrk 1040	83.1 ± 0.4[x]	1.6 ± 0.5	1.0 ± 0.9[x]	16.7 ± 3.2	1.4 ± 0.5	0.8 ± 0.9[x]
Mrk 595	20.5 ± 0.8	2.7 ± 0.2	1.6 ± 0.2	10.7 ± 0.4	2.3 ± 0.2	1.4 ± 0.2
3C 120	23.4 ± 1.5	2.5 ± 0.3[x]	1.4 ± 0.2	18.2 ± 2.3	1.7 ± 0.3[x]	1.0 ± 0.2
Ark 120	18.4 ± 0.2[x]	$\ldots$	$\ldots$	13.1 ± 0.1[x]	$\ldots$	$\ldots$
Mrk 376	13.6 ± 1.2	2.3 ± 0.8[x]	1.4 ± 0.4	14.9 ± 1.5	1.9 ± 0.8[x]	1.2 ± 0.4
Mrk 79	37.4 ± 4.5	1.8 ± 0.3	0.9 ± 0.3	18.1 ± 1.7	1.6 ± 0.3	0.7 ± 0.3
Mrk 382	20.5 ± 0.7	1.8 ± 0.3	0.8 ± 0.2	13.7 ± 0.5	1.5 ± 0.3	0.7 ± 0.2
NGC 3227	127.3 ± 1.0[x]	2.4 ± 0.4[x]	1.9 ± 0.3[x]	10.8 ± 0.1[x]	2.4 ± 0.4[x]	1.9 ± 0.3[x]
NGC 3516	57.7 ± 4.5	$\ldots$	1.0 ± 0.4	10.2 ± 0.8	$\ldots$	0.9 ± 0.4
NGC 4051	181.9 ± 5.5[a,x]	2.4 ± 0.9[x]	$\ldots$	9.9 ± 0.3[a,x]	2.3 ± 0.9[x]	$\ldots$
NGC 4151	101.1 ± 1.7	2.0 ± 0.5	1.3 ± 0.5	8.3 ± 0.3	1.9 ± 0.5	1.3 ± 0.5
Mrk 766	30.3 ± 1.0	2.0 ± 0.2	1.3 ± 0.2	8.0 ± 0.2	1.9 ± 0.2	1.3 ± 0.2
Mrk 771	13.0 ± 0.8	$\ldots$	0.7 ± 0.4	15.8 ± 0.8	$\ldots$	0.6 ± 0.4
NGC 4593	108.2 ± 8.5	$\ldots$	1.0 ± 0.3	19.5 ± 1.2	$\ldots$	1.0 ± 0.3
Mrk 279	25.7 ± 1.7	1.2 ± 0.2[x]	0.6 ± 0.2[x]	14.1 ± 0.8	1.1 ± 0.2[x]	0.5 ± 0.2[x]
NGC 5506	92.4 ± 1.0[x]	2.0 ± 0.2[x]	1.1 ± 0.2[x]	9.4 ± 0.5	1.8 ± 0.2[x]	1.0 ± 0.2[x]
NGC 5548	47.3 ± 3.3	1.9 ± 0.3	1.3 ± 0.3	16.2 ± 1.1	1.8 ± 0.3	1.2 ± 0.3
Ark 479	17.0 ± 0.9	$\ldots$	1.3 ± 0.2[x]	6.5 ± 0.3	$\ldots$	1.2 ± 0.2[x]
Mrk 506	21.8 ± 0.5	2.3 ± 0.2[x]	1.5 ± 0.2[x]	17.3 ± 0.4	2.1 ± 0.2[x]	1.4 ± 0.2[x]
Mrk 507	10.1 ± 0.9	2.7 ± 0.4	1.6 ± 0.3	10.5 ± 0.4	2.4 ± 0.4	1.5 ± 0.3
3C 382	17.8 ± 2.2	2.4 ± 0.3	1.4 ± 0.3	21.0 ± 2.4	2.0 ± 0.3	1.3 ± 0.3
3C 390.3	11.6 ± 0.6	2.6 ± 0.3	1.4 ± 0.2	14.1 ± 0.7	2.2 ± 0.3	1.3 ± 0.2
NGC 6814	91.4 ± 4.0	2.9 ± 0.2	2.0 ± 0.2	9.7 ± 0.7	2.4 ± 0.2	1.7 ± 0.2
Mrk 509	16.8 ± 0.9	2.6 ± 0.2	1.7 ± 0.1	10.8 ± 0.4	2.3 ± 0.2	1.5 ± 0.1
Mrk 1513	15.3 ± 1.0	$\ldots$	1.1 ± 0.5	16.1 ± 0.9	$\ldots$	1.0 ± 0.5
Mrk 304	11.4 ± 0.5	2.0 ± 0.2	1.3 ± 0.2	15.4 ± 0.6[x]	1.6 ± 0.2	1.1 ± 0.2
Ark 564	23.7 ± 0.2[x]	1.4 ± 0.3[x]	1.0 ± 0.3[x]	10.9 ± 0.1[x]	1.2 ± 0.3[x]	0.9 ± 0.3[x]
NGC 7469	49.4 ± 1.1	1.9 ± 0.2	1.2 ± 0.1	14.5 ± 0.3	1.7 ± 0.2	1.1 ± 0.1
Mrk 315[b]	14.5 ± 0.8	2.1 ± 0.6	1.0 ± 0.4	12.9 ± 1.8	1.5 ± 0.6	0.7 ± 0.4
NGC 7603	41.1 ± 0.2	$\ldots$	1.1 ± 0.3	21.6 ± 1.2	$\ldots$	1.0 ± 0.3
Mrk 541	18.9 ± 2.3	$\ldots$	1.1 ± 0.2	12.3 ± 1.7	$\ldots$	0.9 ± 0.2
Med./MAD	$\ldots$	$2.2 / 0.4$	$1.3 / 0.2$	$13.9 / 3.7$	$1.9 / 0.3$	$1.1 / 0.3$

[a] The 25 B mag arcsec^{-2} isophote was used.

[b] Chatzichristou's (2000) images available through NED were used.

[x] The SMA or CI were extrapolated; the extrapolated SMA and CI were not taken into account in the weight-averaging of multi-epoch data unless all the data are extrapolated.

Table 4 Bar parameters, estimated in I_C, except for the galaxies, for which HST or 2MASS data were used.

Galaxy	PA_{bar} (degree)	ϵ_{bar}	$\epsilon_{\mathrm{bar}}^{(i)}$	$\ell_{\max}$ (arcsec)	ℓ (arcsec)	$\ell^{(i)}$ (arcsec)	(kpc)	$\ell^{(i)}/a_{24}^{(0)}$
Mrk 352[a,b]	176.9 ± 2.0	0.158 ± 0.010	0.34 ± 0.02	2.0 ± 0.2	2.2 ± 0.1	2.8 ± 0.1	0.75 ± 0.03	0.18 ± 0.01
Mrk 573	178.5 ± 1.7	0.339 ± 0.016	0.42 ± 0.01	9.1 ± 0.6	10.2 ± 0.1	11.8 ± 0.3	3.73 ± 0.10	0.36 ± 0.02
Mrk 595	111.2 ± 0.7	0.365 ± 0.008	0.13 ± 0.01	6.5 ± 0.9	8.5 ± 0.2	9.0 ± 0.3	4.57 ± 0.13	0.43 ± 0.02
Mrk 376	9.9 ± 0.3	0.511 ± 0.005	0.39 ± 0.03	4.3 ± 0.3	5.3 ± 0.1	5.8 ± 0.1	6.06 ± 0.12	0.41 ± 0.04
Mrk 79[c]	57.1 ± 0.5	0.596 ± 0.007	0.66 ± 0.03	14.9 ± 1.0	19.4 ± 0.2	22.7 ± 0.6	9.94 ± 0.28	0.55 ± 0.05
Mrk 382	5.6 ± 1.3	0.390 ± 0.030	0.33 ± 0.03	6.7 ± 0.3	8.0 ± 0.3	8.4 ± 0.4	5.53 ± 0.25	0.40 ± 0.02
NGC 3227	150.0 ± 2.2	0.603 ± 0.032	0.21 ± 0.08	51.9 ± 6.8	63.3 ± 8.9	63.3 ± 8.9	6.21 ± 0.87	0.57 ± 0.08
NGC 3516	167.8 ± 0.1	0.279 ± 0.001	0.34 ± 0.01	11.8 ± 0.3	14.1 ± 0.1	16.6 ± 0.3	2.98 ± 0.05	0.29 ± 0.02
NGC 4051	134.6 ± 0.7	0.600 ± 0.010	0.45 ± 0.11	60.9 ± 2.9	74.3 ± 5.1	86.2 ± 8.1	5.26 ± 0.49	0.53 ± 0.05
NGC 4151	128.2 ± 0.8	0.510 ± 0.010	0.54 ± 0.02	65.3 ± 3.7	76.5 ± 0.6	81.7 ± 2.7	6.70 ± 0.22	0.81 ± 0.03
Mrk 766	106.0 ± 0.7	0.457 ± 0.009	0.43 ± 0.03	10.1 ± 1.2	13.3 ± 0.2	14.7 ± 0.4	3.99 ± 0.12	0.50 ± 0.02
Mrk 771[a]	30.9 ± 1.3	0.429 ± 0.015	0.44 ± 0.04	5.0 ± 0.4	6.0 ± 0.2	6.6 ± 0.3	7.77 ± 0.31	0.49 ± 0.03
NGC 4593	56.7 ± 0.2	0.627 ± 0.004	0.44 ± 0.14	47.6 ± 4.2	58.1 ± 5.9	60.6 ± 6.5	12.11 ± 1.30	0.62 ± 0.08
Mrk 279[a]	31.1 ± 0.4	0.430 ± 0.004	0.13 ± 0.01	5.6 ± 0.4	7.3 ± 0.3	7.3 ± 0.3	4.29 ± 0.15	0.30 ± 0.02
Ark 479	105.3 ± 0.1	0.474 ± 0.001	0.25 ± 0.02	5.6 ± 0.2	7.2 ± 0.1	7.3 ± 0.1	2.87 ± 0.02	0.44 ± 0.02
NGC 6814[d]	28.0 ± 0.8	0.288 ± 0.006	0.33 ± 0.01	12.1 ± 1.3	15.8 ± 0.1	17.0 ± 0.4	1.51 ± 0.04	0.16 ± 0.01
Ark 564	37.8 ± 1.5	0.460 ± 0.020	0.57 ± 0.01	8.1 ± 0.7	9.3 ± 0.1	11.9 ± 0.2	5.44 ± 0.09	0.50 ± 0.01
NGC 7469	120.4 ± 0.7	0.360 ± 0.010	0.12 ± 0.01	16.0 ± 0.4	18.5 ± 0.2	18.5 ± 0.2	5.47 ± 0.07	0.38 ± 0.01
Med./MAD	…	…	0.39 / 0.12	…	…	…	5.44 / 1.80	0.44 / 0.11

[a] The bar parameters were estimated using archival HST data.
[b] Not taken into account in the computation of the median parameters (see text).
[c] The multi-epoch bar parameters were not weight-averaged.
[d] The bar parameters were estimated using 2MASS data.

Table A1 Log of the observations.

Galaxy	Civil Date (yyyy mm dd)	FWHM (arcsec)	β	Calibration
(1)	(2)	(3)	(4)	(5)
Mrk 1040	1997 09 06	1.36 ± 0.02	2.98 ± 0.19	SS
NGC 5506	1999 04 17	2.51 ± 0.04	…	M 92
Mrk 507	1998 07 20	1.96 ± 0.02	2.45 ± 0.05	M 92

Key to columns. (3) and (4) FWHM (full width at half maximum) and power-law index (β), respectively, of the Moffat PSF (point spread function); ellipsis dots denote Gaussian PSF was assumed; (5) Standard fields used for calibration: SS – secondary standards used.